ELSEVIER

Physica D 97 (1996) 291–310

PHYSICA D

Anomalous diffusion in asymmetric random walks with a quasi-geostrophic flow example

Eric R. Weeks [1], J.S. Urbach, Harry L. Swinney *

Center for Nonlinear Dynamics and Department of Physics, University of Texas at Austin, Austin, TX 78712, USA

Abstract

We present a model of one-dimensional symmetric and asymmetric random walks. The model is applied to an experiment studying fluid transport in a rapidly rotating annulus. In the model, random walkers alternate between flights (steps of constant velocity) and sticking (pauses between flights). Flight time and sticking time probability distribution functions (PDFs) have power law decays: $P(t) \sim t^{-\mu}$ and $t^{-\nu}$ for flights and sticking, respectively. We calculate the dependence of the variance exponent γ ($\sigma^2 \sim t^\gamma$) on the PDF exponents μ and ν. For a broad distribution of flight times ($\mu < 3$), the motion is superdiffusive ($1 < \gamma < 2$), and the PDF has a divergent second moment, i.e., it is a Lévy distribution. For a broad distribution of sticking times ($\nu < 3$), either superdiffusion or subdiffusion ($\gamma < 1$) can occur, with qualitative differences between symmetric and asymmetric walks. For narrow PDFs ($\mu > 3$, $\nu > 3$), normal diffusion ($\gamma = 1$) is recovered. Predictions of the model are related to experimental observations of transport in a rotating annulus. The Eulerian velocity field is chaotic, yet it is still possible to distinguish between well-defined sticking events (particles trapped in vortices) and flights (particles making long excursions in a jet). The distribution of flight lengths is well described by a power law with a divergent second moment (Lévy distribution). The observed transport is strongly asymmetric and is well described by the proposed model.

1. Introduction

1.1. Random walks

A wide range of diffusive processes can be interpreted as random walks. For example, the Brownian motion of a passive particle in a homogenous fluid is described as a sequence of steps generated by random collisions with fluid molecules. As Einstein [1] showed, an ensemble of such particles will spread out with a variance

$$\sigma^2(t) = \langle x^2(t)\rangle - \langle x(t)\rangle^2 = 2Dt, \tag{1}$$

where D is the diffusion coefficient. The broad applicability of this simple result is a consequence of the Central Limit Theorem (CLT): a collection of sums of a large number of statistically independent events will be Gaussian distributed, provided that the distribution of the individual event sizes is not too broad. As applied to random walks, the CLT implies that whenever the mean time between steps and the mean square step size (second moment of the step size distribution) are finite, normal diffusion will result.

In general, anomalous diffusion ($\sigma^2 \propto t^\gamma$ with $\gamma \neq 1$) in physical systems is a consequence of correlations generated by spatial or temporal coherence,

* Corresponding author.
E-mail: swinney@chaos.ph.utexas.edu.
[1] E-mail: weeks@chaos.ph.utexas.edu.

0167-2789/96/$15.00 Copyright © 1996 Elsevier Science B.V. All rights reserved
PII S0167-2789(96)00082-6

and the associated breakdown of the assumptions of the CLT [2,3]. It is often still possible to describe the transport in terms of a random walk, with broad distributions of step sizes or waiting times accounting for the correlations in the motion. For a distribution $P(l)$ of step sizes l given by $P(l) \propto l^{-\mu}$ with $\mu < 3$, the second moment is divergent, and the CLT is no longer applicable. The long excursions which result in a divergent second moment are called Lévy flights. The presence of Lévy flights usually leads to anomalous diffusion. Quantitative connections between the behavior of the distribution functions and the exponent γ have been made for symmetric random walks [4–9].

In this paper we consider *asymmetric*, or biased, one-dimensional random walks, where steps in one direction occur with a higher probability than steps in the opposite direction. This can occur in situations such as charged particles moving in an electric field, or particles carried by an asymmetric flow. We will examine the case of flights with finite velocity. (Some authors use the term Lévy walks for motions with constant velocity and reserve flights for instantaneous jumps.) When the CLT applies, it is always possible to shift to a reference frame where $v_{\text{ave}} = 0$, and the presence of asymmetry only affects the diffusion coefficient, not the exponent ($\gamma = 1$). When the CLT is not applicable, we find that the asymptotic behavior for symmetric and asymmetric random walks can be quite different.

The model we present examines anomalous diffusion arising from random walks with discrete steps of constant velocity, separated by pauses (sticks) of random duration. Asymmetric random walks of this form were used to model the first experimental observations of anomalous diffusion (of electrons in amorphous materials) [10,11], and were studied theoretically for cases with broad distributions of sticking times (but with narrow distributions for flight lengths) [8]. We consider power law forms for both sticking and flight distribution functions, and provide the first comprehensive analysis of the relationship between γ and the sticking and flight distribution exponents for both symmetric and asymmetric random walks. Several other mechanisms can lead to anomalous diffusion, e.g., when the successive discrete steps of a random walk have strong correlations [2]. Also, random walks occurring in a random environment can lead to ultraslow diffusion ($\sigma^2(t) \sim (\ln t)^\alpha$, $\alpha > 0$) [12,13]. Fractional Brownian motion, a generalization of Brownian motion that leads to anomalous diffusion, was proposed by Mandelbrot and Van Ness [14]. As in regular Brownian motion, individual steps cannot be resolved. A comprehensive review of other mechanisms leading to anomalous diffusion can be found in [2].

1.2. Transport in fluid flows

A collection of particles in a nonuniform flow will disperse as a consequence of the shear in the velocity field as well as the effects of molecular diffusion. In most situations, advection due to fluid motion is much faster than molecular diffusion, and large scale structures, such as eddies, jets, or convection rolls, will dominate the transport. This results in correlations in particle velocities for large distances and/or times, and can lead to a failure of the assumptions of the CLT. In fully developed turbulence, for example, the presence of eddies distributed over many spatial scales results in superdiffusion ($\sigma^2 \propto t^\gamma$, $\gamma > 1$), and Richardson [15] argued that the separation of two particles in the atmosphere is described by $\sigma^2 \propto t^3$.

Extremely long time transport of passive tracer particles in fluid flow will be normally diffusive due to Brownian motion [16]. However, for many important flows this time scale is enormously large; for example, in oceanic flows typical length scales are $L \approx 10$ km; for a diffusion constant $D \approx 10^{-5}$ cm^2/s, the diffusive time scale is $\tau_d = L^2/D \approx 10^9$ yr, while time scales of interest are typically ~ 1 yr. In this paper we present an experimental investigation of transport in a rotating fluid flow consisting of a circular chain of vortices bounded by a jet. The motion of tracer particles in the flow is naturally described as a one-dimensional random walk, alternating between motion in the jet corresponding to steps, and waiting times between steps while the particles are trapped in the vortices. Since particles move between vortices almost exclusively in the jet, the motion is strongly asymmetric. The measured distribution of the step sizes is well described by a power law with

exponent less than three; thus the steps are Lévy flights.

Previous work on symmetric random walks is discussed in Section 2. In Section 3, we introduce a continuous time random walk model which allows for asymmetric motion, showing that in some cases the growth of the variance is different from the symmetric results. Section 4 discusses our experimental system, and in Section 5 we present observations of strongly asymmetric Lévy flights. Appendix A defines the notations used in this paper, and Appendix B contains a discussion of additional details of the model.

2. Anomalous diffusion and Lévy flights

2.1. Theory

For simple cases, the variance of an ensemble of random walkers grows linearly with time, as given by Eq. (1), with the diffusion constant D being given by

$$D = \frac{\langle l^2 \rangle - \langle l \rangle^2}{2T}. \tag{2}$$

The moments of l are based on $P_F(l)$, the distribution of step sizes (or *flight* sizes, as we will use), and T is the mean time between the start of successive flights. This result depends only on the first two moments of the step size Probability Distribution Function (PDF) and finite nonzero T, but no other details of the random walk. The mean position of random walkers is

$$\langle x \rangle = \frac{\langle l \rangle}{T} t, \tag{3}$$

which is zero for a symmetric ($\langle l \rangle = 0$) random walk [2].

For PDFs that decay sufficiently slowly, the CLT no longer applies. If $P_F(|l|) \sim |l|^{-\mu}$ and $\mu < 3$, the second moment $\langle l^2 \rangle$ is infinite ($\mu > 1$ for the distribution to be normalizable). A random walk for this type of PDF is a Lévy flight, and it has been shown [4–7] that the variance scales with time $\sigma^2(t) \sim t^\gamma$ with

$$\gamma = 2, \qquad 1 < \mu < 2, \tag{4}$$

$$\gamma = 4 - \mu, \qquad 2 < \mu < 3, \tag{5}$$

$$\gamma = 1, \qquad \mu > 3. \tag{6}$$

In addition, for $\mu = 2$ the variance grows as $t^2/\ln t$, and for $\mu = 3$ the variance grows as $t \ln t$ [7]. These results are valid when the random walker moves at constant velocity, taking flights with a length distribution given by $P_F(|l|)$, or equivalently, a distribution of flight times having the same asymptotic power law behavior. In addition, the time T must be finite. Superdiffusive transport, $1 < \gamma < 2$, occurs for $2 < \mu < 3$. When $\gamma = 2$, the transport is ballistic, that is, the exponent is the same as that of a collection of particles moving in different directions in straight lines, with no pauses or changes in direction.

To consider cases where $T \to \infty$, we allow the random walker to pause (stick) between steps, and introduce the sticking time distribution (also called "trapping" distribution). Again, we assume the behavior at large times decays as a power law: $P_S \sim t^{-\nu}$. When $\nu < 2$ (with $\nu > 1$ for normalization), $\langle t_s \rangle$ (the first moment of the sticking PDF) is infinite and the variance has the possibility of scaling subdiffusively. Shlesinger [8] investigated the case where random walkers were stuck for varying times between random (symmetrically chosen) steps with finite mean square step size ($\mu > 3$), finding

$$\gamma = 1, \qquad \nu > 2, \tag{7}$$

$$\gamma = \nu - 1, \qquad 1 < \nu < 2. \tag{8}$$

Shlesinger [8] also considered random walks with asymmetric steps ($\langle l \rangle \neq 0$) and found the scaling of the mean, $\langle x \rangle \sim \langle l \rangle t^\beta$ with

$$\beta = 1, \qquad \nu > 2, \tag{9}$$

$$\beta = \nu - 1, \qquad 1 < \nu < 2, \tag{10}$$

and the scaling of the variance, $\sigma^2 \sim t^\gamma$, with

$$\gamma = 4 - \nu, \qquad 2 < \nu < 3, \tag{11}$$

$$\gamma = 2\nu - 2, \qquad 1 < \nu < 2. \tag{12}$$

In the asymmetric case, the possibility for superdiffusion exists with broad sticking PDFs. For example, when $\nu = 2.5$, $\gamma = 4 - 2.5 = 1.5$. This will be discussed further in Section 3. Asymmetric random walks of this type describe transport of electrons in amorphous materials [10,11], where the asymmetry is introduced by a bias voltage.

The case with power law sticking PDFs combined with symmetric Lévy flights was examined by Klafter and Zumofen [9] who found for flights with constant velocity

$$\gamma = 2 + \nu - \mu, \quad \nu < 2, \quad 2 < \mu < 3, \tag{13}$$

$$\gamma = 4 - \mu, \quad \nu > 2, \quad 2 < \mu < 3, \tag{14}$$

where Eq. (14) is the same as Eq. (5). This formula allows for the behavior to be subdiffusive ($\gamma < 1$) for sufficiently small values of ν ($1 < \nu < \mu - 1$).

Random walks with a broad sticking and flight distributions can be found in Hamiltonian systems. Sticking behavior is usually associated with island chains near closed, ordered regions of phase space, while flights occur between island chains or in chaotic jets [3,17,18]. The distributions were found to be well described by power laws for both sticking [17–21] and flights [6,21,22]. In some cases, sticking events in a map representation are equivalent to flights in the full phase space [6,22–24]. Maps with power law sticking behavior [17,25] and flight behavior [26] appear to be common. Transport in Hamiltonian systems can be either normal or anomalous, depending on the structure of the phase space [27–29].

Two-dimensional incompressible fluid flow (of the type discussed in Section 5) is related to Hamiltonian systems, as the equations of motion for particle trajectories are equivalent to Hamilton's equations with the streamfunction $\psi(x, y, t)$ taking the place of the Hamiltonian [30]: $dx/dt = \partial\psi/\partial y$, $dy/dt = -\partial\psi/\partial x$. For time-dependent streamfunctions, particles can follow chaotic trajectories, resulting in *chaotic advection* (corresponding to Hamiltonian chaos) [30,31]. This can occur even when the flow is time periodic (laminar). Previous experimental work measured both sticking and flight time PDFs, including flows exhibiting Lévy flights and anomalous diffusion, and found agreement with the results discussed above (Eqs. (4)–(6) and (13), (14)) [32].

2.2. Experiments

Several experimental studies of transport have observed anomalous diffusion. Subdiffusion has been observed in both linear and planar arrays of vortices of alternating sign [33–35]. The results have been interpreted as a simple random walk comprised of sticking and flight events [33]. Particles carried by capillary waves were found to move superdiffusively [36,37], linked to the fractional Brownian motion of the particle trajectories. Tracers in the ocean showed evidence of superdiffusion, although lack of statistics prevented the study of underlying mechanisms [38]. In addition, experiments studying mixing of polymer-like micelles found that transport was superdiffusive, and well described by a Lévy flight model [39,40], although direct observation of flight motions was not possible. In addition to fluid experiments, anomalous diffusion has been observed in photoconductivity of amorphous materials [10,11] and motion of low density lipoprotein receptors on the surface of human skin fibroblasts [41]. Lévy flights also appear in an analysis of sub-recoil laser cooling of atoms [42,43], where the mean time for atoms to leave an optical trap is infinite.

3. Asymmetric random walks

In results such as Eqs. (4)–(6) and (13), (14), the random walk was assumed to be symmetric ($P_F(l) = P_F(-l)$). In the absence of left-right symmetry, many of these results change. For example, if the flights are exclusively in one direction ($P_F(l) = 0$ when $l < 0$), the sticking occurrences will appear as flights in the opposite direction when viewed from a reference frame centered on $\langle x(t) \rangle$ (which might not be moving at constant velocity; e.g., Table 3). In cases such as this the divergence of the second moment of the sticking PDF can lead to superdiffusive behavior (Eq. (11)), because the sticking events will be Lévy flights as seen in the moving reference frame.

In this section we use a model based on a one-dimensional random walk to predict the asymptotic scaling of the variance: as $t \to \infty$, $\sigma^2(t) \sim t^\gamma$. The goal is to find the dependence of γ on the parameters of the model, and to examine differences between symmetric and asymmetric random walks.

3.1. Model

Consider a particle that alternates between sticking events (remaining at the same location for some period of time), and constant velocity flights (moving to the left ($-x$ direction) or the right ($+x$)). The velocity of the leftward flights is v_l, and the rightward v_r. ($v_l > 0$ means motion to the left, and $v_r > 0$ means motion to the right.) The probability of a leftward flight is p_l; rightward, $p_r = 1 - p_l$. The particles originally start at the origin $x = 0$, and at time $t = 0$ start flight events with probability p_F^0 or sticking events with probability $p_S^0 = 1 - p_F^0$.

Both flight and sticking events are of random duration. The probability distribution function (PDF) for flights in either direction is given by the function $P_F(t)$:

$$P_F(t) = \begin{cases} 0, & t < t_F, \\ At^{-\mu}, & t \geq t_F, \end{cases} \tag{15}$$

where t_F is a cutoff at short times to allow the function to be normalizable; the normalization constant is $A = (\mu - 1)t_F^{\mu-1}$. Similarly, the sticking PDF is given by the function $P_S(t)$:

$$P_S(t) = \begin{cases} 0, & t < t_S, \\ Bt^{-\nu}, & t \geq t_S \end{cases} \tag{16}$$

with $B = (\nu - 1)t_S^{\nu-1}$. The scaling exponent γ of the variance only depends on the asymptotic behavior of the sticking and flight PDFs (the exponents μ and ν), although some results that follow will depend slightly on the exact behavior at short times; this will be clarified later. This particular short time behavior was chosen for convenience in comparison with experimental results (see Section 5).

Our goal is to find the PDF $X(x, t)$ of the particle positions for long times, following a procedure similar to that of Ref. [5]. From this PDF we can calculate the variance $\sigma^2(t) = \langle x^2(t)\rangle - \langle x(t)\rangle^2$, and extract the scaling exponent γ. The moments of x are obtained from the Fourier transform of X:

$$(i^n)\frac{\partial^n \tilde{X}(k,t)}{\partial k^n}\bigg|_{k=0} = \langle x^n \rangle. \tag{17}$$

We construct $\tilde{X}(k, t)$ from simpler PDFs related to the particle motion. Let $\xi(x, t)$ be the probability that a flight event has a distance of x and a duration of t:

$$\xi(x,t) = [p_r\delta(x - v_r t) + p_l\delta(x + v_l t)]\, P_F(t). \tag{18}$$

The Dirac delta functions ensure that the flights are made with the correct constant velocity. Define $\Psi(x, t)$ to be the probability that the particle has moved a distance x in time t in a single flight event, and possibly is still moving:

$$\Psi(x,t) = [p_r\delta(x - v_r t) + p_l\delta(x + v_l t)] \int_t^\infty d\tau\, P_F(\tau). \tag{19}$$

Similarly for sticking events, $\Phi(t)$ is the probability that the particle has been motionless for at least duration t and possibly will remain motionless:

$$\Phi(t) = \int_t^\infty d\tau\, P_S(\tau). \tag{20}$$

In addition, we define two functions related to X. Let $Y(x, t)$ be the probability of just starting a sticking event at x, t and $Z(x, t)$ be the probability of just starting a flight event at x, t. Then

$$Y(x,t) = p_S^0\delta(x)\delta(t) + \int_{-\infty}^{\infty} dx' \int_0^t dt'\, Z(x',t')\xi(x - x', t - t'), \tag{21}$$

$$Z(x,t) = p_F^0\delta(x)\delta(t) + \int_0^t dt'\, Y(x',t')P_S(t - t'). \tag{22}$$

The delta functions represent the initial conditions at $t = 0$. The integrals evaluate the probability of being at the correct location earlier, and then having moved to (or stayed at) the current location to begin the sticking

or flight event. $X(x,t)$ can be defined in terms of these new functions, and we get

$$X(x,t) = \int_0^t dt' \, \Phi(t-t') Y(x,t') + \int_{-\infty}^{\infty} dx' \int_0^t dt' \, \Psi(x-x', t-t') Z(x',t'). \tag{23}$$

$X(x,t)$ is the probability of getting stuck at location x at an earlier time t' multiplied by the probability of still being stuck there now (at time t), added to the probability of starting a flight somewhere earlier (at x', t') multiplied by the probability of flying to location x now.

The integral equations can be solved by Fourier transforming in space and Laplace transforming in time. Thus:

$$\begin{aligned}\tilde{X}(k,s) &= \tilde{\Phi}(s)\tilde{Y}(k,s) + \tilde{\Psi}(k,s)\tilde{Z}(k,s) \\ &= \left[s^{-1}(1-\tilde{P}_S)\right]\left[\frac{p_S^0 + p_F^0 \tilde{\xi}(k,s)}{1-\tilde{\xi}(k,s)\tilde{P}_S}\right] \\ &\quad + \left[p_r \tilde{\lambda}(s_r) + p_l \tilde{\lambda}(s_l)\right]\left[\frac{p_S^0 + p_S^0 \tilde{\xi}(k,s)}{1-\tilde{\xi}(k,s)\tilde{P}_S}\right],\end{aligned} \tag{24}$$

where $s_l = s - ikv_l$, $s_r = s + ikv_r$ (each of the four terms in square brackets [ ] corresponds to one of the terms in the previous line). The function $\tilde{\lambda}$ has been introduced for convenience:

$$\tilde{\lambda}(s) = s^{-1}(1 - \tilde{P}_F(s)). \tag{25}$$

Note that

$$\tilde{\xi}(k,s) = p_r \tilde{P}_F(s_r) + p_l \tilde{P}_F(s_l). \tag{26}$$

At this point $\tilde{X}(k,s)$ has been completely expressed in terms of the Laplace transforms of the two elementary PDFs for flight and sticking events, $\tilde{P}_F(s)$ and $\tilde{P}_S(s)$.

Using Eq. (17), we obtain $\langle x \rangle$ and $\langle x^2 \rangle$ by taking derivatives of $\tilde{X}(k,s)$:

$$\langle x \rangle = \frac{v_{ave}(p_F^0 + p_S^0 \tilde{P}_S)(1-\tilde{P}_F)}{s^2(1-\tilde{P}_F\tilde{P}_S)}, \tag{27}$$

$$\begin{aligned}\langle x^2 \rangle = 2\big[&v_{rms}^2(1-\tilde{P}_F + s\tilde{P}_F')(1-\tilde{P}_F\tilde{P}_S) \\ &+ v_{ave}^2 \tilde{P}_S(\tilde{P}_F - 1)s\tilde{P}_F'\big] \\ &\times \frac{(p_F^0 + p_S^0\tilde{P}_S)}{s^3(1-\tilde{P}_F\tilde{P}_S)^2},\end{aligned} \tag{28}$$

where $v_{ave} = p_r v_r - p_l v_l$ and $v_{rms} = \sqrt{p_r v_r^2 + p_l v_l^2}$. If v_{ave} is set to zero, the expressions provide the behavior for a symmetric random walk. The results in Eqs. (27) and (28) are exact for any form of $P_F(t)$ and $P_S(t)$; no approximations have been made.

3.2. Results

The asymptotic behavior of $\langle x(t) \rangle$ and $\langle x^2(t) \rangle$ at large t (small s) can be obtained from an expansion of Eqs. (27) and (28) in powers of s. The Laplace transforms of $P_F(t)$ and $P_S(t)$ (Eqs. (15) and (16)) are

$$\tilde{P}_F(s) = As^{\mu-1}\Gamma(1-\mu, st_F), \tag{29}$$

$$\tilde{P}_S(s) = Bs^{\nu-1}\Gamma(1-\nu, st_S) \ . \tag{30}$$

Expanding the incomplete Gamma function for small arguments yields

$$\tilde{P}_F(s) = -\Gamma(2-\mu)t_F^{\mu-1}s^{\mu-1} + 1 - \langle t_f \rangle s + \frac{1}{2!}\langle t_f^2 \rangle s^2 - \frac{1}{3!}\langle t_f^3 \rangle s^3 \ldots \tag{31}$$

with a similar result for $\tilde{P}_S(s)$. The expression in terms of the moments of the PDFs is correct only for these particular PDFs.

We begin with the symmetric case, $v_{ave} = 0$, so that $\langle x \rangle = 0$ and the variance $\sigma^2(t) = \langle x^2(t) \rangle$. The asymptotic behavior is found by putting the expansions into Eq. (28) and keeping only the leading term. The results, summarized in Fig. 1(a) and Table 1, are in the form $\sigma^2(t) = C(v_{rms})^2 t^\gamma$. Fig. 1(a) shows the asymptotic diffusive behavior in the form of a phase diagram with the different shadings representing the ballistic, superdiffusive, normal, and subdiffusive regimes. The transitions from one phase to another that occur as the exponents of the PDFs are varied are sharply defined only in the infinite time limit.

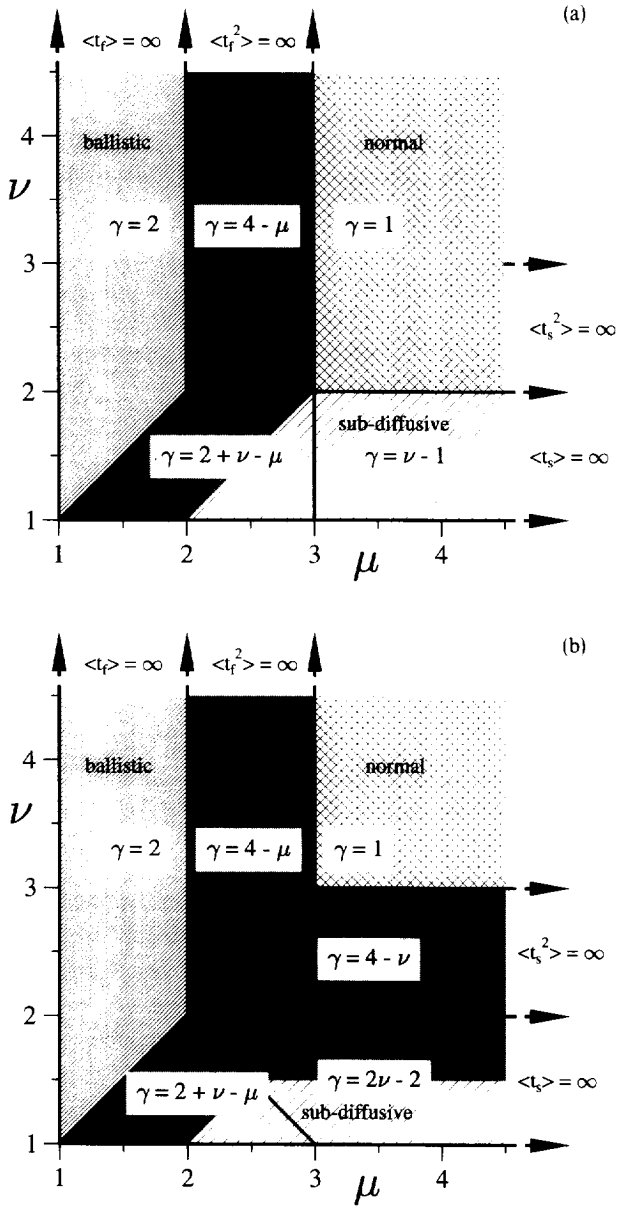

Fig. 1. Phase diagrams for variance of (a) symmetric and (b) asymmetric (or biased) random walks. μ and ν are the exponents controlling the asymptotic power law decay of the flight and sticking PDFs, respectively: $P_F(t_f) \sim t_f^{-\mu}$ and $P_S(t_s) \sim t_s^{-\nu}$, as $t \to \infty$. For each region, bordered by the solid lines, the relationship between the variance exponent γ [$\sigma^2(t) \sim t^\gamma$] and μ and ν is shown. The shadings indicate areas where the behavior is normally diffusive ($\gamma = 1$), subdiffusive ($\gamma < 1$), superdiffusive ($\gamma > 1$), and ballistic ($\gamma = 2$).

The results for the exponent γ are in agreement with the earlier work discussed in Section 2. In addition we calculate the coefficients of the power law terms which are also presented in Table 1.

The behavior displayed in Fig. 1 can be understood in terms of the underlying behavior of the random walker. In all cases the variance is directly proportional to $(v_{rms})^2 = p_l v_l^2 + p_r v_r^2$, and this is the only dependence on p_l or p_r and v_l or v_r (assuming $v_{ave} = p_r v_r - p_l v_l = 0$). For the case of normal diffusion, $\mu > 3$ and $\nu > 2$, $\gamma = 1$ and $C = \langle t_f^2 \rangle / (\langle t_f \rangle + \langle t_s \rangle)$. Writing $\langle t_f^2 \rangle v_{rms}^2 = \langle l^2 \rangle$ and $\langle t_s \rangle + \langle t_f \rangle = T$ reproduces the result for Brownian motion, Eqs. (1) and (2). When the flight PDF exponent μ becomes less than three, $\langle l^2 \rangle$ diverges and the behavior becomes superdiffusive. When $\langle |l| \rangle$ diverges as well, we have the limiting case of ballistic motion. (In this case, $\langle t_f \rangle$ and therefore T also has diverged, but the implication of this is that

Table 1
Anomalous diffusion results for symmetric random walks

Conditions		Exponent γ	Coefficient C
$\mu > 3$	$\nu > 2$	1	$\left(\frac{\langle t_f^2\rangle}{\langle t_f\rangle+\langle t_s\rangle}\right)$
$2 < \mu < 3$	$\nu > 2$	$4-\mu$	$\left(\frac{2}{(4-\mu)(3-\mu)}\right)\left(\frac{t_F^{\mu-1}}{\langle t_f\rangle+\langle t_s\rangle}\right)$
$1 < \mu < 2$	$\nu > \mu$	2	$2-\mu$
$\mu > 3$	$1 < \nu < 2$	$\nu - 1$	$\left(\frac{1}{\Gamma(2-\nu)\Gamma(\nu)}\right)\langle t_f^2\rangle t_S^{1-\nu}$
$\nu < \mu < 3$	$1 < \nu < 2$	$2+\nu-\mu$	$\left(\frac{2\Gamma(3-\mu)}{\Gamma(2-\nu)\Gamma(3-\mu+\nu)}\right) t_F^{\mu-1} t_S^{1-\nu}$

Note: The variance scales asymptotically as $\sigma^2(t) \sim Ct^\gamma v_{\rm rms}^2$ ($v_{\rm rms} = (p_l v_l^2 + p_r v_r^2)^{1/2}$), with coefficient C and exponent γ listed in the table for different values of the flight PDF exponent μ and the sticking PDF exponent ν. γ is correct for any PDF with the same asymptotic scaling, while the values shown for C are correct only for the specific form of the PDFs with the cutoff times t_F and t_S (Eqs. (15) and (16)). Terms such as $\langle t_f\rangle$ and $\langle t_s\rangle$ are the moments of the flight and sticking PDFs, respectively.

Table 2
Scaling of the mean position for asymmetric random walks

Conditions		β	Coefficient K
$\mu > 2$	$\nu > 2$	1	$\frac{\langle t_f\rangle}{\langle t_s\rangle+\langle t_f\rangle}$
$1 < \mu < 2$	$\nu > \mu$	1	1
$\mu > 2$	$1 < \nu < 2$	$\nu - 1$	$\left(\frac{\mu-1}{(\mu-2)\Gamma(2-\nu)\Gamma(\nu)}\right) t_F t_S^{1-\nu}$
$1 < \mu < 2$	$1 < \nu < \mu$	$1+\nu-\mu$	$\left(\frac{\Gamma(2-\mu)}{\Gamma(2-\nu)\Gamma(2-\mu+\nu)}\right) t_F^{\mu-1} t_S^{1-\nu}$

Note: $v_{\rm ave} = p_r v_r - p_l v_l \neq 0$, $\langle x\rangle \sim K v_{\rm ave} t^\beta$. β is correct for any PDF with the same asymptotic scaling, while the values shown for K are correct only for the specific form of the PDFs (Eqs. (15) and (16)). μ is the exponent for the decay of the flight PDF, and ν for the sticking PDF.

the flight motion dominates the transport completely, leading to ballistic motion.) Likewise, when the sticking PDF exponent ν becomes less than 2, T becomes infinite because of the divergence of $\langle t_s\rangle$, leading to subdiffusive behavior as the transport is inhibited. For both $\mu < 3$ and $\nu < 2$, competition between the Lévy flights and the sticking leads to behavior that can be either subdiffusive or superdiffusive, depending on which process is stronger (see Fig. 1(a)).

For the case when $v_{\rm ave} \neq 0$, we first compute the asymptotic behavior of the mean $\langle x\rangle \sim K v_{\rm ave} t^\beta$ using Eq. (27). The results are presented in Table 2. Again, these results can be interpreted through the underlying PDFs. In all cases the mean is proportional to $v_{\rm ave}$, which contains all of the relevant information about the asymmetry. When $\mu > 2$ and $\nu > 2$, $\langle l\rangle$ is finite and the mean grows linearly with time, at a rate given by $K v_{\rm ave} = \langle l\rangle / T$. When $\langle l\rangle$ becomes infinite ($\mu < 2$), T also diverges and the ratio $\langle l\rangle / T$ is equivalent to $v_{\rm ave}$. As predicted in Section 1, when the sticking PDF has an infinite first moment, behavior becomes more complicated, with the result that the mean grows slower than linearly in time.

The results for the variance in the asymmetric case are presented in Table 3 and Fig. 1(b). The phase boundaries are significantly different from the symmetric case. The result in the region of normal diffusion ($\mu > 3, \nu > 3$) is once again equivalent to Eqs. (1) and (2), with $\langle l^2\rangle$ having a more complicated form because of the asymmetry. When either μ or ν is between 2 and 3, the resulting superdiffusion can be thought of as arising from a Lévy flight mechanism. For $2 < \mu < 3$, the flights are Lévy flights; for $2 < \nu < 3$, when shifting to a reference frame moving at constant velocity (equal to $\langle t_f\rangle / (\langle t_f\rangle + \langle t_s\rangle)$; see Table 2), sticking events appear as Lévy flights moving "backwards" with the speed of the moving reference frame. Ballistic motion occurs in the same region

Table 3
Anomalous diffusion results for asymmetric random walks

Conditions		γ	Coefficient C
$\mu > 3$	$\nu > 3$	1	$\left[\frac{\langle t_f\rangle^2(\langle t_s^2\rangle+\langle t_f^2\rangle)-2\langle t_f\rangle^2\langle t_s\rangle^2}{T^3}\right] v_{ave}^2 + \frac{\langle t_f^2\rangle}{T}\left[v_{rms}^2 - \frac{2\langle t_f\rangle}{T} v_{ave}^2\right]$
$2 < \mu < 3$	$\nu > \mu$	$4-\mu$	$\frac{2}{(4-\mu)(3-\mu)}\left[v_{rms}^2 - \frac{(T+\langle t_s\rangle)\langle t_f\rangle}{T^2} v_{ave}^2\right]\left(\frac{t_F^{\mu-1}}{T}\right)$
$\mu > \nu$	$2 < \nu < 3$	$4-\nu$	$\frac{2}{(4-\nu)(3-\nu)}\left(\frac{t_S^{\nu-1}\langle t_f\rangle^2}{T^3}\right) v_{ave}^2$
$1 < \mu < 2$	$\nu > \mu$	2	$(2-\mu)\left(v_{rms}^2 - v_{ave}^2\right)$
$\mu > 4-\nu$	$1 < \nu < 2$	$2\nu - 2$	$\left(\frac{2\Gamma^2(\nu)-\Gamma(2\nu-1)}{\Gamma^2(2-\nu)\Gamma^2(\nu)\Gamma(2\nu-1)}\right)\langle t_f\rangle^2 t_S^{2-2\nu} v_{ave}^2$
$\nu < \mu < 4-\nu$	$1 < \nu < 2$	$2+\nu-\mu$	$\left(\frac{2\Gamma(3-\mu)}{\Gamma(2-\nu)\Gamma(3-\mu+\nu)}\right) t_F^{\mu-1} t_S^{1-\nu} v_{rms}^2$

Note: $v_{ave} = p_r v_r - p_l v_l \neq 0$, $\sigma^2 \sim Ct^\gamma$ with the coefficients C and exponent γ given in the table. T is defined to be $\langle t_s\rangle + \langle t_f\rangle$. μ is the exponent for the decay of the flight PDF, and ν for the sticking PDF. γ is correct for all PDFs with the same asymptotic scaling, while the values shown for C are correct only for the specific form of the PDFs (Eqs. (15) and (16)).

as the symmetric case, for similar reasons. When $1 < \nu < 2$, motion can be either super- or sub-diffusive. For larger values of ν in this range, motion is dominated by the "backwards" Lévy flight mechanism. For smaller values, $\langle x\rangle$ grows too slowly (see Table 2), and the divergence of T leads to subdiffusion.

3.3. Discussion

3.3.1. Exponential PDFs

Exponential PDFs, either sticking or flight, are common in physical situations. In this case, all moments are finite, and the PDF can be treated as a power law with $\mu \to \infty$ or $\nu \to \infty$. If *both* flight and sticking PDFs have exponential tails, the CLT applies, and the behavior is normally diffusive.

For random walks with exponential sticking PDFs, there is no difference between symmetric and asymmetric random walks in the asymptotic transport behavior, and the results of Eqs. (4)–(6) (e.g., $\gamma = 4-\mu$ when $1 < \mu < 2$) apply. Random walks without sticking events can be treated in the same way (all moments are finite and equal to zero) and again Eqs. (4)–(6) describe the behavior as a function of μ. The mean of asymmetric random walks when the sticking PDF is exponential grows linearly in time ($\langle r\rangle \sim v_{ave} t$) for all values of μ.

Exponential flight PDFs can lead to different behavior, depending on the symmetry. If $2 < \nu < 3$, asymmetric random walks are superdiffusive while symmetric walks are normally diffusive, as seen in Section 3.2. The case where "flights" are actually steps of constant length, as has been considered previously [2], is equivalent to exponential flight PDFs – again, the important aspect is that all moments of the flight PDF are finite, and again, asymptotic behavior depends on the presence or absence of symmetry.

3.3.2. Higher dimensions

The results can be easily extended to higher dimensions. The variance in higher dimensions can be broken up into components:

$$\sigma^2 = \langle \boldsymbol{r}\cdot\boldsymbol{r}\rangle - \langle \boldsymbol{r}\rangle\cdot\langle \boldsymbol{r}\rangle = \sigma_x^2 + \sigma_y^2 + \sigma_z^2 \tag{32}$$

in three dimensions, for example. If flights are taken in a random (symmetrically chosen) angular direction with flight distance described by a power law PDF, the results of the previous section with $v_{ave} = 0$ hold (although the coefficients may be somewhat different). The results for $v_{ave} \neq 0$ apply if a higher-dimensional asymmetric random walk can be broken up into cartesian components.

3.3.3. Correlated random walks

Our results have been derived for independent steps and pauses. For cases where the steps are correlated, the results can be different (for example, if all the steps are in the same direction for a given random walker, or if all pauses are the same length). In some cases, random walks with short-range correlations can be treated as random walks with uncorrelated steps on a longer time scale. In this way the results for the asymptotic behavior can still apply. This approach is discussed in [2].

4. Experimental system

We now describe an experimental study of transport that yields an asymmetric random walk. An annular tank (Fig. 2) rigidly rotates at 1.0 Hz (6.28 rad/s) (the geometry with a flat-lid and sloping bottom are described more fully in [44]). The lid is flat and the bottom has a gentle slope; the depth ranges from 17.1 cm at the inner radius (r_{in} = 10.8 cm) to 20.3 cm at the outer radius (r_{out} = 43.2 cm); the slope is for the Beta effect used to model the curvature of planets in previous geophysical experiments [45]. An annular ring with inner radius 10.8 cm, outer radius 19.4 cm, and height 6.0 cm is placed on the bottom of the annulus. Because of the rapid rotation, the Taylor–Proudman theorem ensures that the velocity field will be two-dimensional [45,46] except for thin boundary layers at the top and bottom (Ekman layers) and near the vertical walls (Stewartson layers).

Fluid is pumped through two concentric rings of 120 small holes (diameter 0.26 cm), in through a ring at r = 18.9 cm and out through a ring at r = 27.0 cm. As a consequence of the radial pumping, a strong azimuthal jet traveling in the counter-rotating direction ("westward") is produced between the rings of forcing holes. The fluid between the outflow ring of holes and the outer wall is motionless for low pumping rates. Fluid above the annular ring must also be motionless, by the Taylor–Proudman theorem.

For moderate pumping rates, the instability of the shear layer between the azimuthal jet and the motionless fluid results in a chain of vortices above the forcing holes [45]. Against the annular ring, the inner shear layer is a Stewartson boundary layer, which remains stable. In the data presented here, fluid is pumped at a rate of 52.0 cm^3/s, resulting in four large vortices (Fig. 3). At this pumping rate, the motion of the vortices is chaotic, as shown in the velocity power spectra (measured by a hot film probe placed at r = 35.1 cm) in (Fig. 4).

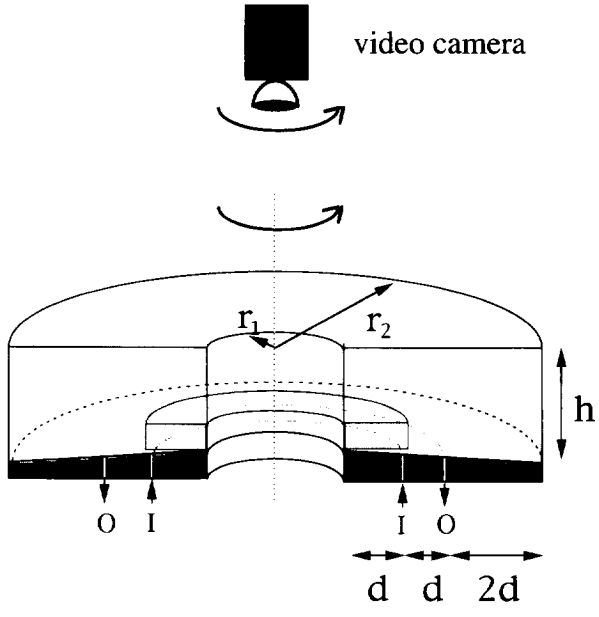

Fig. 2. Sketch of the rotating annulus. Water (kinematic viscosity 0.009 cm^2/s) is pumped in through one ring of holes (marked I), and out through another ring of holes (marked O). The experiment is viewed through a video camera rotating above the experiment.

Transport is measured by putting several hundred small (~ 1 mm diameter), neutrally buoyant tracer particles into the tank. They are illuminated by light shining through the outer cylinder of the annulus and are viewed through a video camera rotating above the experimental set up. Automated tracking techniques [47] are used to find the trajectories of all the particles visible in the flow (usually 5–40 at a time). Individual particles can be tracked for times up to 1000 s; particles are lost when they drift to the inside or outside of the annulus, or if they drift vertically out of the illuminated region. As discussed in Section 2, small passive scalar particles in two-dimensional incompressible fluid flow

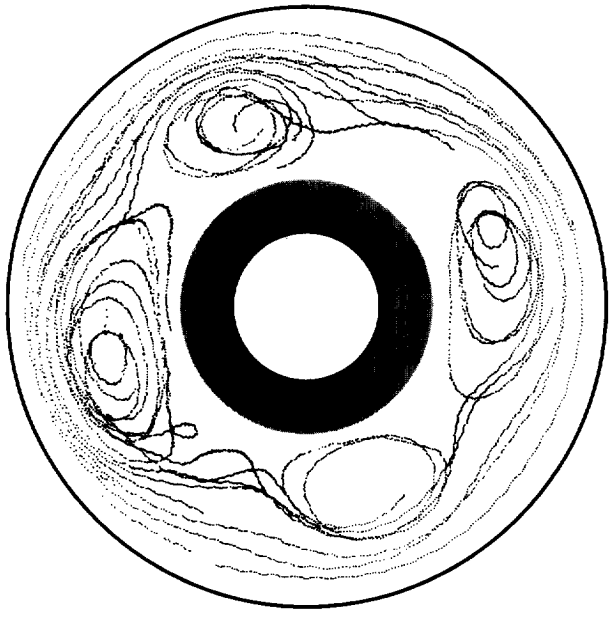

Fig. 3. Streaks formed by 100 s long trajectories of 12 particles reveal the presence of four vortices. The inner and outer circles represent the annulus boundaries, and the grey ring represents the annular barrier.

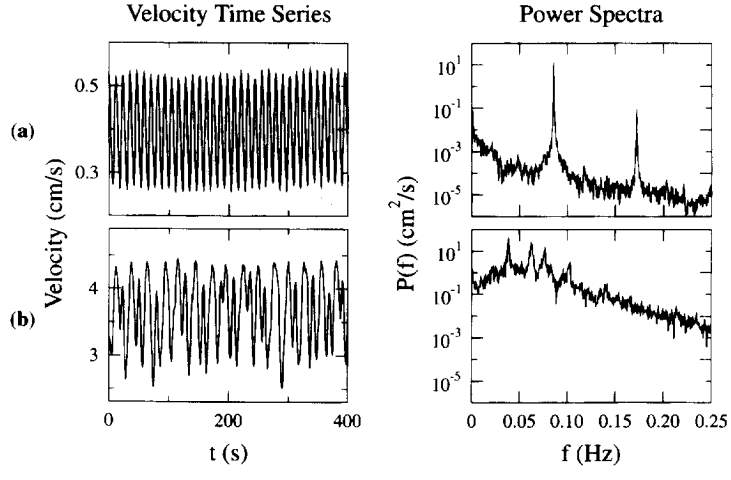

Fig. 4. Velocity time series and power spectra for (a) a time periodic flow (from [48], not discussed in this paper), and (b) chaotic flow, corresponding to Fig. 3. The noise floor in (b) is more than two orders of magnitude larger than in (a).

obey Hamilton's equations of motion, with the streamfunction as the Hamiltonian.

Previous experiments [32,48,49] have used a different forcing configuration, pumping fluid in through the inner ring and out through the outer ring at $r = 35.1$ cm; this also produces a vortex chain. Physical perturbations [48] have resulted in quasi-periodic (see Fig. 3) and chaotic velocity fields, while high pump rates [49] have previously been studied only with quasi-periodic velocity fields. Unlike previous work, in the current experiments the Eulerian chaos arises due to natural instabilities and not due to the presence of a physical perturbation [48].

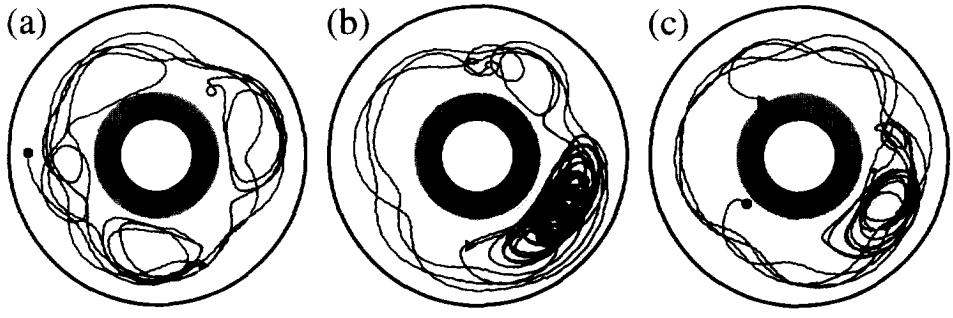

Fig. 5. Trajectories of three tracer particles. The beginning of each trajectory is marked with a triangle, the end with a circle. Nearly all of the flight behavior is in the outer jet; a brief flight in the inside can be seen in (a). The chaotic motion of the four vortices can be seen in (b), where the particle spends most of its time in the same vortex which moves erratically.

5. Results

Trajectories of the individual particles (Figs. 5 and 6) reveal complicated motion. The vortices are advected by the jet, so that in the reference frame of the tank they move in the counter-rotating direction. In the reference frame of the vortex chain, the fluid outside the vortex chain, which is nearly motionless with respect to the annulus, appears as a jet in the opposite (co-rotating) direction. Fig. 5 shows the trajectories of three particles as they alternate between times sticking inside one of the vortices and flight motions in the outer jet. (The co-rotating direction is $+\theta$.) The four vortices are not stationary but move erratically. (The pictures shown are taken in a frame of reference co-rotating with the *average* speed of the vortex chain, but there is substantial variation in the *instantaneous* speed of each vortex.)

Figure 6 shows the angular position of the particles as a function of time. The oscillatory behaviors correspond to motion when the particle is "sticking" in a vortex, and the longer diagonal lines are flights in the outer jet. Flights are distinguished from sticking motions by examining the azimuthal distance traveled before reversing direction: particles travel in a vortex for at most $\frac{1}{2}\pi$ rad before changing directions, while a particle that leaves one vortex and enters the next (the minimum flight distance) will move at least $\frac{1}{2}\pi$ rad. Unlike previous experiments [32,48,49], there is no strong inner jet and particles do not travel long distances on the inner

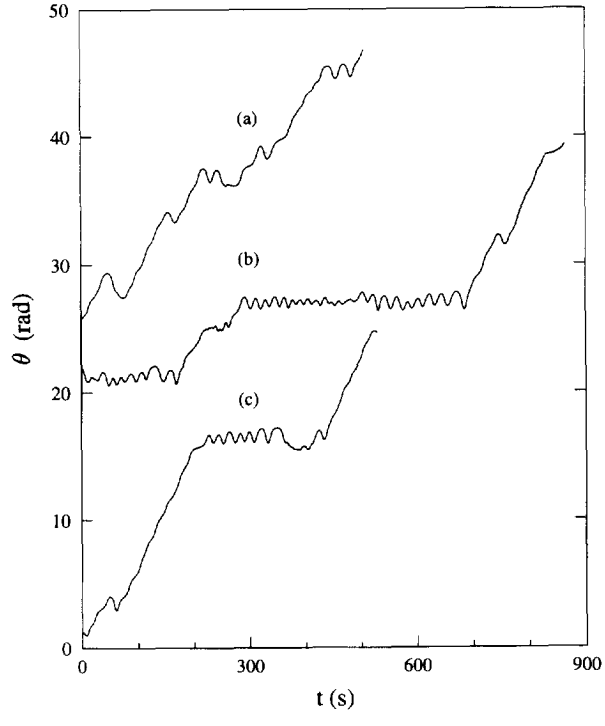

Fig. 6. Angular displacement $\theta(t)$ as a function of time for the trajectories shown in Fig. 5. Diagonal lines indicate flights, while the small oscillations correspond to particle motion within a vortex. Despite the chaotic motion of the vortices, a clear distinction can be made between flight behavior and sticking behavior.

side of the vortex chain. Approximately 10% of the flights seen in the experiment are short hops on the inner side of the vortex chain, from one vortex to an adjacent vortex; these hops take less

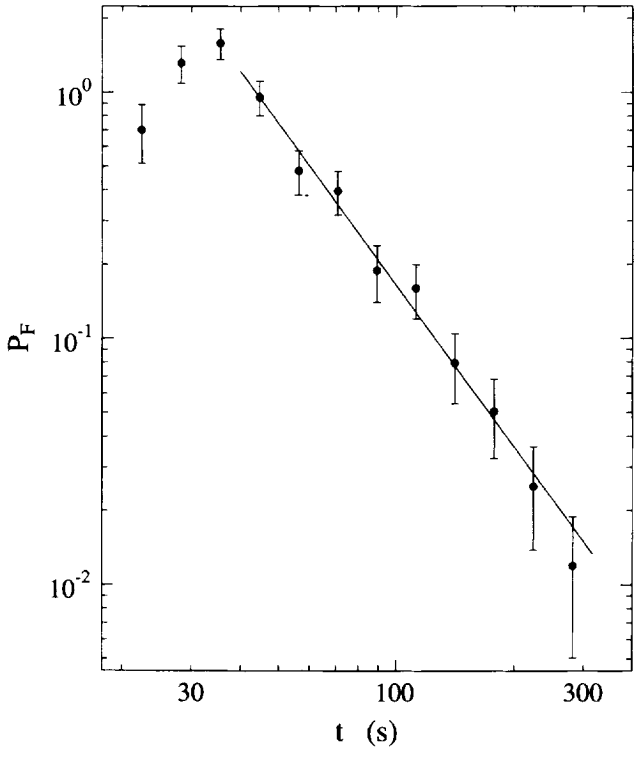

Fig. 7. Flight probability distribution function, showing power law decay with exponent $\mu = 2.2 \pm 0.1$. The error bars show the statistical uncertainty ($\sqrt{N}$). The value of μ, corrected for finite trajectory durations (cf. footnote 2), is $\mu = 1.9 \pm 0.2$.

than 40 s, and do not contribute to the long time statistics.

The PDF for the flight times shows a power law decay, $P_F(t) \sim t^{\mu}$, with $\mu = 1.9 \pm 0.2$ (Fig. 7).[2] As $\mu < 3$, the flight motions correspond to Lévy flights. Previous work [32,48,49] has found power law flight behavior in a variety of flows. What is remarkable in the current work is that the power law behavior exists despite the presence of Eulerian chaos. Although the vortices are moving erratically with respect to each other, particle motion still displays the effects of long time correlations. The sticking time PDF shown in Fig. 8 also shows a broad distribution of time scales. The long term transport can be deduced from the model presented in Section 3: taking $\nu = 1.3$ and $\mu = 1.9$ the variance should grow as t^{γ} with $\gamma = 2 + \nu - \mu \approx 1.4$. While all similar flows we have studied have clear power law decays of the flight PDFs, the sticking PDF behavior is sometimes unclear [48,49]. In some cases it appears that there is a crossover to exponential decay at very long times. If the tail of the sticking PDF shown is exponential, then we would expect $\gamma \approx 2$ (see discussion at the end of Section 3). More data are needed to resolve the behavior of the sticking PDF at long times.

The experimentally determined variance for this flow is shown in Fig. 9 (see [48] for a description of the variance calculation). It is difficult to track particles for long enough times in this flow to gather the statistics necessary to determine the variance accurately;

[2] To obtain the exponents μ and ν from the PDFs, we must correct the measured slope of the PDFs on log–log plots. The measured exponents come from experimental trajectories with finite durations, and are different from the exponents which would be measured from data of infinite duration. We create artificial data with known power law decay, truncate the data to make finite artificial trajectories (with times chosen from the experimental data), and construct PDFs from the artificial data which are compared with the actual data. These corrected exponents are the ones discussed in the text.

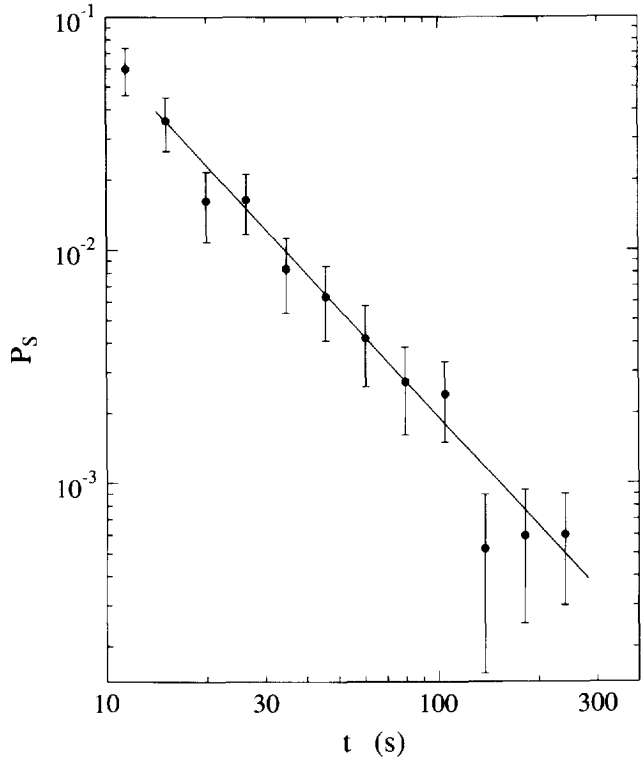

Fig. 8. Sticking probability distribution function. A fit to the data yields a slope of -1.5 ± 0.2 (solid line). The value of ν, corrected for finite trajectory durations (cf. footnote 2), is $\nu = 1.3 \pm 0.2$.

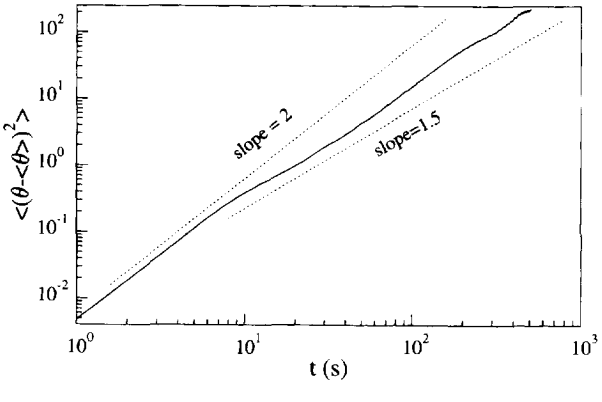

Fig. 9. Variance $\sigma^2(t)$ for the ensemble of tracer particles (solid line).

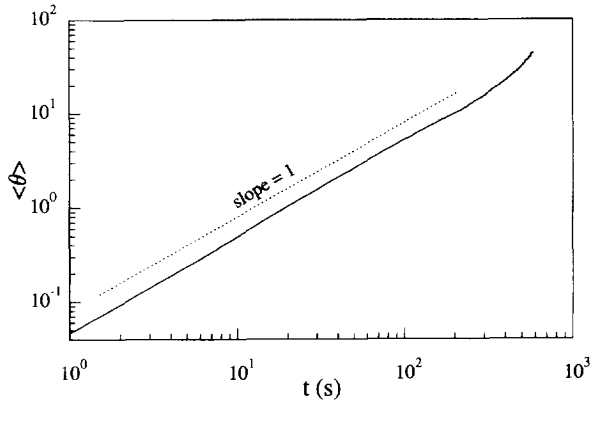

Fig. 10. Mean particle position, $\langle\theta(t)\rangle$ (solid line).

hence quantitative comparison with the results of Section 3 is difficult. However, the behavior is clearly superdiffusive with an exponent γ between 1.5 and 2.0.

The failure of the variance to reach its asymptotic behavior despite the large number of long time trajectories can be understood from an analysis of crossover times in the model. The time necessary to approach the asymptotic state can be calculated by retaining lower-order terms in the expansion for σ (see Appendix B for details). Using the experimental values of $\mu = 1.9$, $\nu = 1.3$, and cutoff times

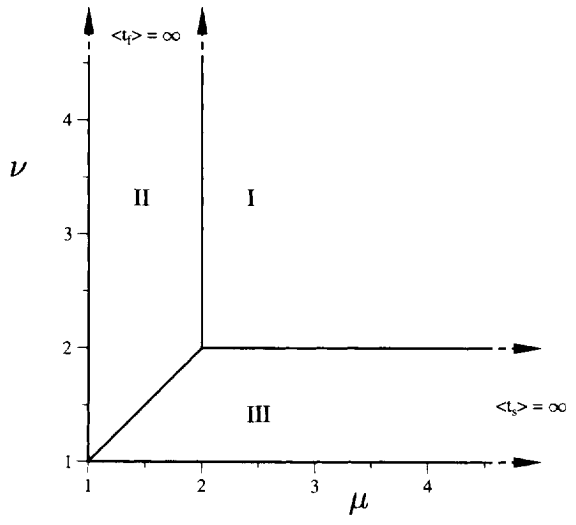

Fig. 11. (a) Phase diagram for the tables in Appendix B. The regions shown correspond to the regions discussed in Tables 5–7. The axes are the flight exponent μ and sticking exponent ν.

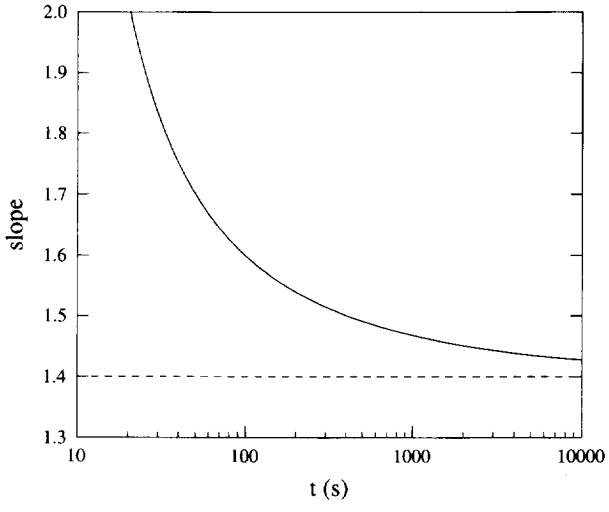

Fig. 12. Graph of slope of the function $Ct^{\gamma} + C't^{\gamma'}$ for $\gamma = 1.40$, $\gamma' = 1.05$, corresponding to the predictions of the model for $\mu = 1.95$, $\nu = 1.35$ measured from the experiment (after corrections due to finite time effects; see Section 5). The constants are $C = 0.055$ and $C' = -0.10$ (from Table 7, with $p_l = 0$, $p_r = 1$, $v_{rms}^2 = v_{ave}^2 = 0.0058$ rad/s, $t_F = 22$ s, $t_S = 10$ s, and $P_S^0 = P_F^0 = 0.5$). There is a broad region with changing slope.

$t_F = 22$ s, $t_S = 10$ s, yields $\sigma \sim 0.055t^{1.4} - 0.10t^{1.1}$. A plot of this function on a log–log scale (Fig. 12) does not reach a slope of 1.5 until 400 s, and our data only extend to $\sim$ 500 s. This slow convergence to asymptotic behavior is a generic feature of Lévy processes and complicates analysis in many experimental situations and numerical simulations.

Fig. 10 shows that the mean particle position $\langle x \rangle$ grows approximately linearly with time for most of the range. For longer times, $\langle x \rangle$ appears to start growing faster than linearly in time. For times less than a vortex turnover time, linear growth is expected, as all particles are moving with constant velocity (whether in a vortex or in the jet). For longer times, the model predicts (for $\mu = 1.9$ and $\nu = 1.3$) that $\langle x \rangle \sim t^{0.4}$; if the sticking PDF has an exponential tail, $\langle x \rangle \sim t$. It is probable that the asympotic scaling is not reached due to lack of statistics at long times (see discussion in Appendix B).

6. Conclusions

When the CLT is applicable, symmetry considerations do not affect the asymptotic diffusive behavior of random walks. However, when the sticking time PDF has an infinite first moment, the transport is subdiffusive for the symmetric case and either sub- or super-diffusive for the asymmetric case. In cases with Lévy flights (divergent second moment of the flight PDF), an arbitrarily small amount of asymmetry or bias can change the asymptotic behavior from subdiffusive to superdiffusive, as discussed in Section 3.

Our experimental results demonstrate the need to consider asymmetry. Transport in the experiment is a result of competition between trapping in the vortices and motion in the jet, which carries particles between vortices for long distances in one direction only. Good qualitative agreement is found between experimental transport and the transport predicted based on the flight and sticking PDFs.

Acknowledgements

The authors are happy to acknowledge their deep debt to Fritz Busse, whose extensive theoretical,

Table 4
List of common symbols used in this paper

Symbol	Meaning
T	Mean time between the start of successive steps
t_F, t_S	Minimum time for short flight, sticking events (see Eqs. (15) and (16))
$\langle t_f \rangle$, $\langle t_s \rangle$	first moment of flight, sticking PDFs
μ	Power law decay exponent for the flight PDFs (see Eq. (15))
ν	Power law decay exponent for the sticking PDFs (see Eq. (16))
γ	Variance exponent: $\sigma^2 \sim t^\gamma$
P_F^0, P_S^0	Probability that first event is a flight event, sticking event
p_l, p_r	Probability a flight is to the left ($-x$), right ($+x$)
v_l, v_r	Velocity in left direction, right direction ($v_l > 0$ for leftward motion)

numerical, and experimental work has set the standard for understanding instability phenomena in fluid dynamics. The senior author (HLS) first learned about convective instabilities from the landmark Clever and Busse paper [50] and has been inspired by Fritz's work and has enjoyed interacting with him for the past two decades.

For the present paper the authors acknowledge helpful discussions with J. Klafter, M.F. Shlesinger, and G.M. Zaslavsky. This work was supported by the Office of Naval Research Grant No. N00014-89-J-1495. ERW acknowledges the support of an ONR Augmentation Award for Science and Engineering Training.

Appendix A. Notation

Table 4 contains a summary of the important notations used in this paper. For a random walk alternating between flight events and sticking events, $T = \langle t_f \rangle + \langle t_s \rangle$ when both moments are finite ($\mu > 2$, $\nu > 2$).

Table 5
Scaling of the mean position for asymmetric random walks

Region	Exponent β	Coefficient K
I	1	$\langle t_f \rangle / T$
	$3-\mu$	$\frac{\langle t_s \rangle t_F^{\mu-1}}{(3-\mu)(2-\mu)T^2}$
	$3-\nu$	$\frac{\langle t_f \rangle t_S^{\nu-1}}{(3-\nu)(2-\nu)T^2}$
	0	$\frac{2\langle t_f \rangle \langle t_s \rangle (P_F^0 \langle t_f \rangle - P_S^0 \langle t_s \rangle) + \langle t_s^2 \rangle \langle t_f \rangle - \langle t_s \rangle \langle t_f^2 \rangle}{2T^2}$
II	1	1
	$\mu-1$	$\frac{-\langle t_s \rangle t_F^{1-\mu}}{\Gamma(2-\mu)\Gamma(\mu)}$
	$1+\mu-\nu$	$-\left(\frac{\Gamma(2-\nu)}{\Gamma(2-\mu)\Gamma(2+\mu-\nu)}\right) t_F^{1-\mu} t_S^{\nu-1}$
III	$\nu-1$	$\left(\frac{\mu-1}{(\mu-2)\Gamma(2-\nu)\Gamma(\nu)}\right) t_F t_S^{1-\nu}$
	$1+\nu-\mu$	$\left(\frac{\Gamma(2-\mu)}{\Gamma(2-\nu)\Gamma(2-\mu+\nu)}\right) t_F^{\mu-1} t_S^{1-\nu}$
	$2\nu-3$	$-\left(\frac{1}{\Gamma^2(2-\nu)\Gamma(2\nu-2)}\right)\left(\langle t_f \rangle + \frac{\nu-1}{\nu-2} t_S\right) \langle t_f \rangle t_S^{2-2\nu}$
	$1-2\mu+2\nu$	$-\left(\frac{\Gamma^2(2-\mu)}{\Gamma^2(2-\nu)\Gamma(2-2\mu+2\nu)}\right) t_F^{2\mu-2} t_S^{2-2\nu}$
	$2-\mu$	$\left(\frac{P_S^0}{\mu-2}\right) t_F^{\mu-1}$
	0	$-P_S^0 \langle t_f \rangle$

Note: $v_{ave} = p_r v_r - p_l v_l \neq 0$, $\langle x \rangle \sim K v_{ave} t^\beta + K' v_{ave} t^{\beta'}$. The terms have been calculated to second order for each region shown in Fig. 11. To use this table, determine which two terms have the largest exponent for a given value of μ and ν. The term with the third largest exponent is not necessarily the third-order term, as the calculations have only been done to second order. In this table T is defined as $\langle t_s \rangle + \langle t_f \rangle$. Terms containing $\langle t_f \rangle$ are only valid for $\mu > 2$, and terms containing $\langle t_s \rangle$ are only valid for $\nu > 2$.

Table 6
Anomalous diffusion results for symmetric random walks

Region	Exponent γ	Coefficient C
I	1	$\frac{\langle t_f^2\rangle}{T}$
	$4-\mu$	$\left(\frac{2}{(4-\mu)(3-\mu)}\right)\frac{t_F^{\mu-1}}{T}$
	$6-2\mu$	$\left(\frac{-2\Gamma(3-\mu)\Gamma(2-\mu)}{\Gamma(7-2\mu)}\right)\left(\frac{t_F^{2\mu-2}}{T^2}\right)$
	$6-\mu-\nu$	$\left(\frac{-2\Gamma(3-\mu)\Gamma(2-\nu)}{\Gamma(7-\mu-\nu)}\right)\left(\frac{t_F^{\mu-1}t_S^{\nu-1}}{T^2}\right)$
	0	$-\frac{4\langle t_f^3\rangle}{3T}+\left(\frac{\langle t_f^2\rangle}{2T^2}\right)\left[\langle t_f^2\rangle+\langle t_s^2\rangle+2\langle t_s\rangle(P_F^0\langle t_f\rangle-P_S^0\langle t_s\rangle)\right]$
II	2	$2-\mu$
	μ	$\left(\frac{2}{\Gamma(2-\mu)\Gamma(1+\mu)}\right)[(\mu-1)t_F+(\mu-2)\langle t_s\rangle]\,t_F^{1-\mu}$
	$2+\mu-\nu$	$\left(\frac{(2\mu-4)\Gamma(2-\nu)}{\Gamma(2-\mu)\Gamma(3+\mu-\nu)}\right)t_F^{1-\mu}t_S^{\nu-1}$
III	$\nu-1$	$\left(\frac{1}{\Gamma(2-\nu)\Gamma(\nu)}\right)\langle t_f^2\rangle t_S^{1-\nu}$
	$2+\nu-\mu$	$\left(\frac{2\Gamma(3-\mu)}{\Gamma(2-\nu)\Gamma(3-\mu+\nu)}\right)t_F^{\mu-1}t_S^{1-\nu}$
	$2\nu-3$	$\left[\frac{1}{\Gamma(3-\nu)\Gamma(2-\nu)\Gamma(2\nu-2)}\right]((\nu-2)\langle t_f\rangle+(\nu-1)t_S)\,\langle t_f^2\rangle t_S^{2-2\nu}$
	0	$-P_S^0\langle t_f^2\rangle$
	$2\nu-\mu$	$\left[\frac{2\Gamma(3-\mu)}{\Gamma(3-\nu)\Gamma(2-\nu)\Gamma(1-\mu+2\nu)}\right]((\nu-2)\langle t_f\rangle+(\nu-1)t_S)\,t_F^{\mu-1}t_S^{2-2\nu}$
	$3-\mu$	$\frac{2P_S^0}{\mu-3}t_F^{\mu-1}$
	$2+2\nu-2\mu$	$\left(\frac{(2\mu-4)\Gamma^2(2-\mu)}{\Gamma^2(2-\nu)\Gamma(3-2\mu+2\nu)}\right)t_F^{2\mu-2}t_S^{2-2\nu}$

Note: $v_{ave}=p_r v_r-p_l v_l=0$, $\sigma^2\sim Cv_{rms}^2t^\gamma+C'v_{rms}^2t^{\gamma'}$. For each region shown in Fig. 11, the terms for σ^2 have been calculated to second order. See the footnote to Table 5 for an explanation on how to use this table.

Table 7
Anomalous diffusion results for asymmetric random walks

Region	Exponent γ	Coefficient C
I	1	$\left[\frac{\langle t_f\rangle^2(\langle t_s^2\rangle+\langle t_f^2\rangle)-2\langle t_f\rangle^2\langle t_s\rangle^2}{T^3}\right]v_{ave}^2+\frac{\langle t_f^2\rangle}{T}\left[v_{rms}^2-\frac{2\langle t_f\rangle}{T}v_{ave}^2\right]$
	$4-\mu$	$\frac{2}{(4-\mu)(3-\mu)}\left[\left(\frac{-(T+\langle t_s\rangle)\langle t_f\rangle}{T^2}\right)v_{ave}^2+v_{rms}^2\right]\left(\frac{t_F^{\mu-1}}{T}\right)$
	$4-\nu$	$\frac{2}{(4-\nu)(3-\nu)}\left(\frac{t_S^{\nu-1}\langle t_f\rangle^2}{T^3}\right)v_{ave}^2$
	$6-2\mu$	$\left(\frac{2\Gamma(3-\mu)\Gamma(2-\mu)}{\Gamma(7-2\mu)}\right)\left(\frac{t_F^{2\mu-2}}{T^2}\right)\left[\frac{\langle t_f\rangle-\langle t_s\rangle}{T}v_{ave}^2-v_{rms}^2\right]$ $+\left(\frac{t_F^{2\mu-2}}{T^4}\right)\Gamma^2(2-\mu)\left[\frac{2\langle t_s\rangle^2-4\langle t_f\rangle\langle t_s\rangle}{\Gamma(7-2\mu)}-\frac{\langle t_s\rangle^2}{\Gamma^2(4-\mu)}\right]v_{ave}^2$
	$6-2\nu$	$\left(\frac{\Gamma^2(2-\nu)(6\Gamma^2(4-\nu)-\Gamma(7-2\nu))}{\Gamma(7-2\nu)\Gamma^2(4-\nu)}\right)\left(\frac{\langle t_f\rangle^2t_S^{2\nu-2}}{T^4}\right)v_{ave}^2$
	0	$\left[\left(\frac{\langle t_f^2\rangle}{2T^2}\right)\left[\langle t_f^2\rangle+\langle t_s^2\rangle+2\langle t_s\rangle\left(P_F^0\langle t_f\rangle-P_S^0\langle t_s\rangle\right)\right]-\frac{4\langle t_f^3\rangle}{3T}\right]v_{rms}^2$

↓

Table 7
Continue

Region	Exponent γ	Coefficient C
		$+\left(\frac{4}{3T^3}\right)\langle t_f^3\rangle\langle t_f\rangle\,(T+\langle t_s\rangle)\,v_{ave}^2+\left(\frac{4}{3T^3}\right)\langle t_s^3\rangle\langle t_f\rangle^2 v_{ave}^2$
		$+\left(\frac{\langle t_f^2\rangle^2}{4T^4}\right)\left(3\langle t_s\rangle^2-4\langle t_f\rangle\langle t_s\rangle-2\langle t_f\rangle^2\right)v_{ave}^2$
		$+\left(\frac{5\langle t_s^2\rangle\langle t_f\rangle}{4T^4}\right)\left(\langle t_s^2\rangle\langle t_f\rangle-2\langle t_f^2\rangle\langle t_s\rangle\right)v_{ave}^2$
		$+\left(\frac{-P_F^0\langle t_f\rangle^2}{T^4}\right)\left[\langle t_f^2\rangle\langle t_s\rangle(\langle t_f\rangle+3\langle t_s\rangle)+\langle t_f\rangle^2\langle t_s^2\rangle\right]v_{ave}^2$
		$+\left(\frac{\langle t_f\rangle\langle t_s\rangle}{T^4}\right)\Big[\langle t_f\rangle\langle t_s\rangle\left(\langle t_f\rangle^2-4\langle t_f\rangle\langle t_s\rangle-\langle t_s^2\rangle\right)$
		$+3\langle t_f^2\rangle\langle t_s\rangle^2+3\langle t_f\rangle^2\langle t_s^2\rangle\Big]v_{ave}^2-\left(\frac{(P_S^0)^2\langle t_s\rangle^2\langle t_f\rangle^2}{T^2}\right)v_{ave}^2$
		$+\left(\frac{P_S^0\langle t_f\rangle}{T^4}\right)\left[2\langle t_s\rangle^3(\langle t_f\rangle^2+\langle t_f^2\rangle)+\langle t_f\rangle^2\langle t_s^2\rangle\langle t_s\rangle+2\langle t_f\rangle\langle t_s\rangle^4\right]v_{ave}^2$
II	2	$(2-\mu)\left(v_{rms}^2-v_{ave}^2\right)$
	μ	$\left(\frac{2}{\Gamma(2-\mu)\Gamma(1+\mu)}\right)[(\mu-1)t_F+(\mu-2)\langle t_s\rangle]\,t_F^{1-\mu}\left(v_{rms}^2-v_{ave}^2\right)$
	$2+\mu-\nu$	$\left(\frac{2\Gamma(2-\nu)}{\Gamma(2-\mu)\Gamma(3+\mu-\nu)}\right)\left[(4-\mu-\nu)v_{ave}^2+(\mu-2)v_{rms}^2\right]t_F^{1-\mu}t_S^{\nu-1}$
III	$2\nu-2$	$\left(\frac{2\Gamma^2(\nu)-\Gamma(2\nu-1)}{\Gamma^2(2-\nu)\Gamma^2(\nu)\Gamma(2\nu-1)}\right)\langle t_f\rangle^2 t_S^{2-2\nu}v_{ave}^2$
	$2+\nu-\mu$	$\left(\frac{2\Gamma(3-\mu)}{\Gamma(2-\nu)\Gamma(3-\mu+\nu)}\right)t_F^{\mu-1}t_S^{1-\nu}v_{rms}^2$
	$3\nu-4$	$\left(\frac{[2\Gamma(3\nu-3)-4\Gamma(\nu)\Gamma(2\nu-2)][(2-\nu)\langle t_f\rangle+(1-\nu)t_S]}{\Gamma(3-\nu)\Gamma^2(2-\nu)\Gamma(\nu)\Gamma(2\nu-2)\Gamma(3\nu-3)}\right)\langle t_f\rangle^2 t_S^{3-3\nu}v_{ave}^2$
	$\nu-1$	$\left(\frac{1}{\Gamma(2-\nu)\Gamma(\nu)}\right)\left[-\langle t_f\rangle^2 v_{ave}^2+\langle t_f^2\rangle v_{rms}^2\right]t_S^{1-\nu}$
	$3-\mu$	$\frac{2P_S^0}{\mu-3}t_F^{\mu-1}v_{rms}^2$
	$2+2\nu-2\mu$	$\left(\frac{\Gamma^2(2-\mu)((2\mu-2)\Gamma^2(2-\mu+\nu)-\Gamma(3-2\mu+2\nu))}{\Gamma^2(2-\nu)\Gamma^2(2-\mu+\nu)\Gamma^2(3-2\mu+2\nu)}\right)t_F^{2\mu-2}t_S^{2-2\nu}v_{ave}^2$
		$-\left(\frac{2(2-\mu)\Gamma^2(2-\mu)}{\Gamma^2(2-\nu)\Gamma(3-2\mu+2\nu)}\right)t_F^{2\mu-2}t_S^{2-2\nu}v_{rms}^2$

Note: $v_{ave}=p_r v_r-p_l v_l\neq 0$, $\sigma^2\sim Ct^\gamma+C't^{\gamma'}$. For each region shown in Fig. 11, the terms for σ^2 have been calculated to second order. For an explanation on how to use this table, see the footnote to Table 5.

Appendix B. Second-order terms

The asymptotic behavior of $\langle x\rangle$ and $\langle x^2\rangle$ depends only on the leading terms in the expansion of Eqs. (27) and (28). In order to study the approach to the asymptotic limit, it is necessary to calculate higher-order terms. In this appendix, we use Eq. (31) for the expansion of the Laplace transform of the PDFs to produce the second-order terms. The variance will scale in time, generally, as $\sigma^2(t)\sim Ct^\gamma+C't^{\gamma'}$ with $\gamma'<\gamma$. The asymptotic behavior, given in Section 3, will always be given by the largest exponent.

Regions with different second-order terms are shown in Fig. 11. We calculate the highest-order terms for each region; these are listed in Tables 5–7. The calculations are valid to second order, so that while several terms are listed for each of the regions shown in Fig. 11, only the two terms with the largest

exponents are useful. The other terms may have exponents which are smaller than neglected third-order terms that do not appear in the table.

As discussed in Section 5, crossover times must be considered in deducing the anomalous diffusion exponent from data. If the variance σ^2 is given by

$$\sigma^2(t) = at^{\gamma} + bt^{\gamma'}, \quad \gamma > \gamma', \tag{B.1}$$

then the slope on a log–log plot is given by $\mathrm{d}(\ln \sigma^2)/\mathrm{d}(\ln t)$:

$$\text{slope}(t) = \frac{\gamma + \gamma'(b/a)t^{\gamma'-\gamma}}{1 + (b/a)t^{\gamma'-\gamma}}, \tag{B.2}$$

which as $t \to 0$ has the value γ' and as $t \to \infty$ has the value γ, as expected. If $\gamma - \gamma'$ is small, the time to crossover to the asymptotic behavior is very large. For example, in Fig. 12, with $b/a = -1.82$, $\gamma = 1.40$ and $\gamma' = 1.05$, it takes 400 s for the measured exponent to get below 1.5, within 0.1 of the correct asymptotic value. (When b/a is negative, as in Fig. 12, there is a divergence of the slope when the denominator vanishes in Eq. (B.2)).

References

[1] A. Einstein, Über die von der molekularkinetischen Theorie der Wärme geforderte Bewegung von in ruhenden Flüssigkeiten suspendierten Teilchen, Ann. Physik 17 (1905) 549.

[2] J.P. Bouchaud and A. Georges, Anomalous diffusion in disordered media: statistical mechanisms, models and physical applications, Phys. Rep. 195 (1990) 127.

[3] M.F. Shlesinger, G.M. Zaslavsky and J.Klafter, Strange kinetics, Nature 363 (1993) 31; J. Klafter, M.F. Shlesinger and G. Zumofen, Beyond Brownian motion, Physics Today 49 (1996) 33.

[4] M.F. Shlesinger and J. Klafter, Lévy walk representations of dynamics processes, in: Perspectives in Nonlinear Dynamics, eds. M.F. Shlesinger, R. Cawley, A.W. Saenz and W. Zachary (World Scientific, Singapore, 1986) pp. 336–349.

[5] J. Klafter, A. Blumen and M.F. Shlesinger, Stochastic pathway to anomalous diffusion, Phys. Rev. A 35 (1987) 3081.

[6] T. Geisel, A. Zacherl and G. Radons, Chaotic diffusion and 1/f-noise of particles in two-dimensional solids, Z. Phys. (B) 71 (1988) 117.

[7] X.-J. Wang, Dynamical sporadicity and anomalous diffusion in the Lévy motion, Phys. Rev. A 45 (1992) 8407.

[8] M.F. Shlesinger, Asymptotic solutions of continuous-time random walks, J. Stat. Phys. 10 (1974) 421.

[9] J. Klafter and G. Zumofen, Lévy Statistics in a Hamiltonian System, Phys. Rev. E 49 (1994) 4873.

[10] H. Scher and E.W. Montroll, Anomalous transit-time dispersion in amorphous solids, Phys. Rev. B 12 (1975) 2455.

[11] G. Pfister and H. Scher, Dispersive (non-Gaussian) transient transport in disordered solids, Adv. Phys. 27 (1978) 747.

[12] Ya.G. Sinai, The limiting behavior of a one-dimensional random walk in a random medium, Theory Probab. Appl. 27 (1982) 256.

[13] E. Marinari, G. Parisi, D. Ruelle and P. Windey, Random walk in a random environment and 1/f noise, Phys. Rev. Lett. 50 (1983) 1223.

[14] B.B. Mandelbrot and J.W. Van Ness, Fractional Brownian motions, fractional noises and applications, SIAM Rev. 10 (1968) 422.

[15] L.F. Richardson, Atmospheric diffusion shown on a distance-neighbour graph, Proc. Roy. Soc. London Ser. A 110 (1926) 709.

[16] W. Young, A. Pumir and Y. Pomeau, Anomalous diffusion of tracer in convection rolls, Phys. Fluids A 1 (1989) 462.

[17] J.D. Meiss and E. Ott, Markov-tree model of intrinsic transport in Hamiltonian systems, Phys. Rev. Lett. 55 (1985) 2741.

[18] J.D. Meiss and E. Ott, Markov tree model of transport in area-preserving maps, Physica D 20 (1986) 387.

[19] G. Petschel and T. Geisel, Unusual manifold structure and anomalous diffusion in a Hamiltonian model for chaotic guiding-center motion, Phys. Rev. A 44 (1991) 7959.

[20] J.B. Weiss and E. Knobloch, Mass transport and mixing by modulated traveling waves, Phys. Rev. A 40 (1989) 2579.

[21] G.M. Zaslavsky, D. Stevens and H. Weitzner, Self-similar transport in incomplete chaos, Phys. Rev. E 48 (1993) 1683.

[22] T. Geisel, A. Zacherl and G. Radons, Generic 1/f noise in chaotic Hamiltonian dynamics, Phys. Rev. Lett. 59 (1987) 2503.

[23] G.M. Zaslavsky, Fractional kinetic equation for Hamiltonian chaos, Physica D 76 (1994) 110.

[24] C.F.F. Karney, Long-time correlations in the stochastic regime, Physica D 8 (1983) 360.

[25] T. Geisel and S. Thomae, Anomalous diffusion in intermittent chaotic systems, Phys. Rev. Lett. 52 (1984) 1936.

[26] T. Geisel, J. Nierwetberg and A. Zacherl, Accelerated diffusion in Josephson junctions and related chaotic systems, Phys. Rev. Lett. 54 (1985) 616.

[27] V.V. Afanasiev, R.Z. Sagdeev and G.M. Zaslavsky, Chaotic jets with multifractal space-time random walk, Chaos 1 (1991) 143.

[28] A.A. Chernikov, B.A. Petrovichev, A.V. Rogal'sky, R.Z. Sagdeev and G.M. Zaslavsky, Anomalous transport of streamlines due to their chaos and their spatial topology, Phys. Lett. A 144 (1990) 127.

[29] B.A. Petrovichev, A.V. Rogal'sky, R.Z. Sagdeev and G.M. Zaslavsky, Stochastic jets and nonhomogeneous

transport in Lagrangian turbulence, Phys. Lett. A 150 (1990) 391.
[30] H. Aref, Stirring by chaotic advection, J. Fluid Mech. 143 (1984) 1.
[31] J.M. Ottino, Mixing, chaotic advection, and turbulence, Annu. Rev. Fluid Mech. 22 (1990) 207.
[32] T.H. Solomon, E.R. Weeks and H.L. Swinney, Observation of anomalous diffusion and Lévy flights in a two-dimensional rotating flow, Phys. Rev. Lett. 71 (1993) 3975.
[33] O. Cardoso, B. Gluckmann, O. Parcollet and P. Tabeling, Dispersion in a quasi-two-dimensional-turbulent flow: An experimental study, Phys. Fluids 8 (1996) 209.
[34] O. Cardoso and P. Tabeling, Anomalous diffusion in a linear array of vortices, Europhys. Lett. 7 (1988) 225.
[35] O. Cardoso and P. Tabeling, Anomalous diffusion in a linear system of vortices, Eur. J. Mech. B 8 (1989) 459.
[36] R. Ramshankar, D. Berlin and J.P. Gollub, Transport by capillary waves. Part I: Particle trajectories, Phys. Fluids A 2 (1990) 1955.
[37] R. Ramshankar and J.P. Gollub, Transport by capillary waves. Part II: Scalar dispersion and structure of the concentration field, Phys. Fluids A 3 (1991) 1344.
[38] A.R. Osborne, A.D. Kirwan, Jr., A. Provenzale and L. Bergamasco, Fractal drifter trajectories in the Kuroshio extension, Tellus A 41 (1989) 416.
[39] A. Ott, J.P. Bouchaud, D. Langevin and W. Urbach, Anomalous diffusion in "living polymers": A genuine Lévy flight?, Phys. Rev. Lett. 65 (1990) 2201.
[40] J.P. Bouchaud, A. Ott, D. Langevin and W. Urbach, Anomalous diffusion in elongated micelles and its Lévy flight interpretation, J. Phys. II 1 (1991) 1465.
[41] R.N. Ghosh and W.W. Webb, Automated detection and tracking of individual and clustered cell surface low density lipoprotein receptor molecules, Biophys. J. 66 (1994) 1301.
[42] F. Bardou, J.P. Bouchaud, O. Omile, A. Aspect and C. Cohen-Tannoudji, Subrecoil laser cooling and Lévy flights, Phys. Rev. Lett. 72 (1994) 203.
[43] J. Reichel, F. Bardou, M.Ben Dahan, E. Peik, S. Rand, C. Salomon and C. Cohen-Tannoudji, Raman cooling of cesium below 3 nK: New approach inspired by Lévy flight statistics, Phys. Rev. Lett. 75 (1995) 4575.
[44] J. Sommeria, S.D. Meyers and H.L. Swinney, in: Nonlinear Topics in Ocean Physics, ed. A. Osborne (North-Holland, Amsterdam, 1991) p. 227.
[45] T.H. Solomon, W.J. Holloway and H.L. Swinney, Shear flow instabilities and Rossby waves in barotropic flow in a rotating annulus, Phys. Fluids A 5 (1993) 1971.
[46] J. Pedlosky, Geophysical Fluid Dynamics, 2nd Ed. (Springer, New York, 1987).
[47] M.S. Pervez and T.H. Solomon, Long-term tracking of neutrally buoyant tracer particles in two-dimensional fluid flows, Exp. Fluids 17 (1994) 135.
[48] T.H. Solomon, E.R. Weeks and H.L. Swinney, Chaotic advection in a two-dimensional flow: Lévy flights and anomalous diffusion, Physica D 76 (1994) 70.
[49] E.R. Weeks, T.H. Solomon, J.S. Urbach and H.L. Swinney, Observation of anomalous diffusion and Lévy flights, in: Lévy Flights and Related Topics in Physics, eds. M.F. Shlesinger, G.M. Zaslavsky and U. Frisch (Springer, Heidelberg, 1995) pp. 51–71.
[50] R.M. Clever and F.H. Busse, Transition to time-dependent convection, J. Fluid Mech. 65 (1974) 625.